HHS Public Access

Author manuscript

Neuroimage. Author manuscript; available in PMC 2019 January 01.

Published in final edited form as:

Neuroimage. 2018 January 01; 164: 121–130. doi:10.1016/j.neuroimage.2017.03.005.

Investigating the spatiotemporal characteristics of the deoxyhemoglobin-related and deoxyhemoglobin-unrelated functional hemodynamic response across cortical layers in awake marmosets

Cecil Chern-Chyi Yen, **Daniel Papoti**[1], and **Afonso C. Silva**[*]

Cerebral Microcirculation Section, Laboratory of Functional and Molecular Imaging, National Institute of Neurological Disorders and Stroke, National Institutes of Health, Bethesda, MD 20892, USA

Abstract

Blood oxygenation level dependent (BOLD) functional magnetic resonance imaging (fMRI) has become a major tool to map neural activity. However, the spatiotemporal characteristics of the BOLD functional hemodynamic response across the cortical layers remain poorly understood. While human fMRI studies suffer from low spatiotemporal resolution, the use of anesthesia in animal models introduces confounding factors. Additionally, inflow contributions to the fMRI signal become nonnegligible when short repetition times (TRs) are used. In the present work, we mapped the BOLD fMRI response to somatosensory stimulation in awake marmosets. To address the above technical concerns, we used a dual-echo gradient-recalled echo planar imaging (GR-EPI) sequence to separate the deoxyhemoglobin-related response (absolute T_2* differences) from the deoxyhemoglobin-unrelated response (relative S_0 changes). We employed a spatial saturation pulse to saturate incoming arterial spins and reduce inflow effects. Functional GR-EPI images were obtained from a single coronal slice with two different echo times (13.5 and 40.5 ms) and TR = 0.2 s. BOLD, T_2*, and S_0 images were calculated and their functional responses were detected in both hemispheres of primary somatosensory cortex, from which five laminar regions (L1+2, L3, L4, L5, and L6) were derived. The spatiotemporal distribution of the BOLD response across the cortical layers was heterogeneous, with the middle layers having the highest BOLD amplitudes and shortest onset times. ΔT_2* also showed a similar trend. However, functional S_0 changes were detected only in L1+2, with a fast onset time. Because inflow effects were minimized, the source of S_0 functional changes in L1+2 could be attributed to a reduction of cerebrospinal fluid volume fraction due to the functional increase in cerebral blood volume and to unmodeled T_2* changes in the extra- and intra-venous compartments. Caution should be exercised when interpreting laminar BOLD fMRI changes in superficial layers as surrogates of underlying neural activity.

[*]Corresponding author: Afonso C. Silva, Ph.D. Chief, Cerebral Microcirculation Section Laboratory of Functional and Molecular Imaging National Institute of Neurological Disorder and Stroke National Institutes of Health 49 Convent Drive MSC 4478 Bldg. 49 Room 3A72 Bethesda MD 20892-4478 USA Tel: +1-301-402-9703 Fax: +1-301-480-8670 SilvaA@ninds.nih.gov.

[1]Present address: Department of Physics, Universidade Federal do ABC, Santo Andre, Sao Paulo, 09210, Brazil

Keywords

BOLD; brain; marmosets; non-human primates; onset times; somatosensory cortex

Introduction

The blood oxygenation level dependent (BOLD) functional magnetic resonance imaging (fMRI) has proven to be a valuable tool to non-invasively probe various brain areas at a macroscopic scale (Fukuda et al., 2016; Goense et al., 2016). With continued improvement in both spatial and temporal resolution of MRI, BOLD fMRI has recently been applied to study the temporal dynamics of the laminar hemodynamic response and its underlying neural activity in both animal models and humans (Hirano et al., 2011; Jin and Kim, 2008; Siero et al., 2011; Silva and Koretsky, 2002). The distinct function of the six cortical layers is the foundation of interlaminar connections, which form a larger and more complex intracortical network at macroscopic scale (Thomson and Bannister, 2003). However, an in-depth understanding of the spatiotemporal characteristics of the laminar BOLD response is essential to interpret the laminar BOLD response as a function of its underlying neural activity, to optimize the BOLD fMRI protocol, and to realize the spatiotemporal limitations of the BOLD fMRI technique.

Several studies have been conducted that characterize the temporal aspects of laminar BOLD contrast in various brain areas and species. Faster laminar BOLD onset times were reported in cortical layer 4 or 5, followed by layer 6, and then layers 1–3 of somatosensory cortex in anesthetized rats (Silva and Koretsky, 2002; Tian et al., 2010; Yu et al., 2014). Cerebral blood volume or flow is reported to have onset time monotonically increasing by cortical depth in anesthetized rats or cats (Hirano et al., 2011; Jin and Kim, 2008; Norup Nielsen and Lauritzen, 2001). However, the aforementioned animal studies suffered from confounds of general anesthesia, which is known to alter hemodynamic regulation and neuronal response (Liu et al., 2013; Masamoto and Kanno, 2012). On the other hand, BOLD fMRI in humans shows promising results concerning faster BOLD onset times in layers 5–6 of the visual cortex (Siero et al., 2013). Nevertheless, insufficient spatiotemporal resolution causes laminar onset times to be contaminated by partial volume of white matter or pial vessels/cerebrospinal fluid (CSF). Consequently, conscious, awake marmosets were adopted in the current study as a nonhuman primate model to bridge the gap between high-resolution fMRI in small animals and low-resolution fMRI in humans (Hung et al., 2015c; Silva et al., 2011). Marmosets are phylogenetically closer to humans, compared to other small animals (Marmoset Genome and Analysis, 2014), and have one of the highest cortical thickness to brain mass ratios among primates (Sun and Hevner, 2014).

Another issue that commonly appears in high temporal resolution BOLD fMRI experiments is the large inflow contribution in BOLD contrast (Duyn et al., 1994). Inflow might account for more than half of the BOLD contrast when there is not enough time for the MR signal to recover (Glover et al., 1996). To separate the inflow contribution from the real BOLD contrast, a dual gradient-recalled echo planar imaging (GR-EPI) sequence was utilized to isolate spin-spin relaxation time (T_2*) change from non-T_2* change, which contained the

inflow effect manifested as change in spin-lattice relaxation time (T_1) (Speck and Hennig, 1998). The difference in T_2* is presumably proportional to change in the amount of deoxyhemoglobin in the blood and directly related to BOLD contrast (Kim and Ogawa, 2012). In addition, inflow contribution was suppressed by saturating the incoming blood below the circle of Willis in marmosets. Therefore, any remaining non-T_2* signal would be either from outside of the vasculature and/or exceptions in modeling T_2* by dual echoes.

The main goal of the current study was to investigate the spatiotemporal characteristics of the laminar BOLD hemodynamic response function in the primary somatosensory (S1) cortex of awake marmosets. To accomplish our goal, the present study implemented several strategies to avoid shortcomings in prior studies, such as confounding effects of anesthesia, insufficient spatiotemporal resolution, and inflow contribution. Our results show early onset times of laminar BOLD and deoxyHb component in layers 3–4 of S1, whereas the non-deoxyHb component, which was insensitive to T_2* changes, was significant only in layers 1 and 2. The non-deoxyHb component in layers 1 and 2 exhibited a significantly faster onset time when compared to the deoxyHb component. Since inflow contribution was suppressed by saturation of arterial spins below the circle of Willis, this could only be explained by the shrinkage of the cerebrospinal fluid (CSF) compartment due to expansion of the arterial blood compartment. However, CSF partial volume could not fully explain the peak amplitude of the deoxyHb component in layers 1 and 2. The gap could be filled by the contribution of the slower intravenous signal that was not properly modeled by the dual-echo fitting.

Methods

All procedures were approved by the Animal Care and Use Committee of the National Institute of Neurological Disorders and Stroke. Four male adult common marmosets (*Callithrix jacchus*) weighting 350–500 grams and aged 4–5 years old were housed in pairs in dedicated cages and maintained on a diurnal 12-hour light cycle. Their diet consisted of ad libitum Zupreem canned marmoset food, Purina 5040 biscuits, unfiltered water, and P.R.A.N.G. rehydrator. In addition, the animals were fed daily with various fruit and vegetable treats. Prior to being enlisted in the experiments, the marmosets were acclimated to lying in the sphinx position in an MRI-compatible cradle according to a 27-days long acclimatization protocol as described previously (Silva et al., 2011). Briefly, during the first phase, animals were dressed with a dedicated marmoset jacket (Lomir Biomedical, Inc. Malone, NY). The jacket was then attached with plastic zip-ties to a semi-cylindrical plastic cover, which was secured to the cradle using plastic screws. The marmosets were allowed to remain in the sphinx position for incremental periods of time from 15 minutes on day 1 to 90 minutes on day 9. Only marmosets that had behavioral score less than two (mostly quiet, agitated only initially) on day 9 in each phase of the training would advance to next phase. During the second phase, the marmosets were placed again in the MRI-compatible cradle for incremental periods of time while listening to pre-recorded MRI sounds inside a mock MRI tube. During the final phase, the animals' heads were then comfortably restrained by individualized 3D-printed helmets printed to fit each animal's MRI head profiles (Papoti et al., 2013). The custom-built helmets have been demonstrated to effectively minimize head motion without stressing the animals (Belcher et al., 2013; Liu et al., 2013).

fMRI experiments were conducted in a 7T/300 mm horizontal magnet interfaced to an AVANCE AVIII MRI spectrometer (Bruker, Billerica, USA) and equipped with a self-shielded 150 mm ID gradient set capable of generating 450 mT/m within 150 μs (Resonance Research Inc., Billerica, USA). An actively decoupled birdcage coil with an inner diameter of 110 mm was used as transmit coil. Individualized four-channel receive-only phased array coils were designed and embedded inside the custom-built helmets. The coil elements were sized and placed over the somatosensory cortex to maximize the sensitivity of the experiments (Papoti et al., 2013). Functional images were obtained from a single coronal slice using a dual GR-EPI sequence (short echo time (TE1)/long echo time (TE2)/repetition time (TR) = 13.5/40.5/200 ms; nominal flip angle = 26.3°; matrix size = 128×48; in-plane resolution/thickness = 0.25×0.25/1 mm^3). The bandwidth of the frequency encoding was 278 kHz and echo train length was 21.6 ms. An axial spatial saturation pulse was placed slightly above the circle of Willis to reduce the field-of-view and to saturate arterial spins between the neck and the circle of Willis. Slice position was determined by evaluating pilot fMRI data, and prescribed consistently across sessions with respect to the anatomical landmarks such as the anterior and posterior commissures (Liu et al., 2013).

Electrical stimuli of both hands were delivered by two pairs of contact electrode pads (Biopac Systems, Goleta, USA) placed proximal to the wrist, which stimulated the median, ulnar, and radial nerves of the hand. These pads were connected to stimulus isolators (World Precision Instruments, Sarasota, USA) controlled by a custom-built multichannel pulse generator and Presentation software (Neurobehavioral Systems, Berkeley, USA). The number of runs per session was limited by how long the marmosets could stay calm inside the magnet. Sessions with a significant amount of head motion or sessions with only unilateral activation as revealed by real-time AFNI analysis were omitted (Cox et al., 1995). A total of 14 sessions with 5.7±1.4 (mean ± standard deviation) runs per session were obtained from the four marmosets and included in the analysis. Each run consisted of an off-on-off boxcar paradigm containing 32 epochs of a 2 s-long pre-stimulus baseline, followed by a 4 s-long stimulation block, and a 26 s-long post-stimulus recovery period. The first epoch of each run was always discarded for functional analysis to prevent the change of arousal state between scans from influencing the amplitude of the BOLD response. The stimuli consisted of electrical pulses with the following parameters: current intensity 1.5 mA, pulse duration 0.4 ms, and stimulus repetition frequency 50 Hz (Liu et al., 2013). While in the magnet, the animals were continuously monitored by an MR-compatible camera (MRC Systems, Heidelberg, Germany). In addition, a pressure pillow was placed underneath the animals to monitor their respiration as a fail-safe measurement (Biopac Systems, Goleta, USA).

For each scan, the dual GR-EPI images were split into short echo (TE1 = 13.5 ms) and long echo (TE2 = 40.5 ms) images. Motion parameters were estimated from the short echo images with the 3dAllineate from AFNI (Cox and Hyde, 1997) software package, and used to realign both short and long echo images to the middle scan of each session. Motion-corrected TE1 and TE2 images, excluding those with head displacement larger than a half pixel within one TR, were averaged across each session to generate a mean time series of one epoch. Visual examinations were done after the motion correction to ensure the quality of the motion correction. Pixel-by-pixel calculated BOLD, T_2*, and S_0 images were

averaged for each session and fed to the generalized linear model with BLOCK response function of AFNI's 3dDeconvolve to visualize statistical maps. BOLD statistical maps were also used to guide the positioning of the lateral boundaries of the laminar profile. Custom-written MATLAB (MathWorks, Natick, USA) scripts were used to extract the laminar profile from two echo images semi-automatically. First, the gray matter (upper) and white matter (lower) boundaries of the cortex were delineated by manually identifying and connecting voxels of lower signal intensity relative to the cortex in the short echo image, and fitting the boundaries with second order polynomials. The two ends of the boundary curves were confined to areas with significant activation ($t > 1.98$) as shown in Fig. 1a. Then, lines perpendicular to the tangent of every unique point on the gray matter boundary curve were generated. Along these projection lines, coordinates of 16 equal-distance points between gray matter and white matter boundaries were defined (see Fig. 1b, on the left). The average distance between adjacent points along projection lines was 0.12 mm from both hemispheres of all sessions. Finally, the intensity of every depth point was bi-linearly interpolated from raw images and averaged over the same level to produce profiles of 16 laminas.

For each averaged lamina, the time-dependent signals $S_1(t)$ and $S_2(t)$ were defined as short echo (TE1) and long echo (TE2) images, respectively:

$$\begin{aligned} S_1(t) &= S_0(t) e^{TE1/T2*(t)}, \\ S_2(t) &= S_0(t) e^{TE2/T2*(t)}, \end{aligned} \quad \text{eq. 1}$$

where $T_2*(t)$ and $S_0(t)$ are time-dependent functions of T_2* and MR signal at TE = 0, respectively. The temporal evolution of T_2* reflects changes in the amount of deoxyhemoglobin in the blood and is dubbed the deoxyhemoglobin-related (deoxyHb) signal component, whereas the temporal evolution of S_0 reflects changes not related to deoxyhemoglobin and is therefore dubbed the deoxyhemoglobin-unrelated (non-deoxyHb) signal component (Kim and Ogawa, 2012). TE1 (13.5 ms) and TE2 (40.5 ms) were selected so that their mean value was the optimal TE (27 ms) for BOLD contrast at 7T (Siero et al., 2011). Hence, the BOLD signal at optimal TE could be calculated as the geometric mean of $S_1(t)$ and $S_2(t)$:

$$BOLD(t) = S_0(t) e^{(TE1+TE2)/2/T2*(t)} = S_1(t)^{1/2} S_2(t)^{1/2}, \quad \text{eq. 2}$$

Assuming a single compartment mono-exponential decay of the MRI signal, T_2* (deoxyHb component), and S_0 (non-deoxyHb component) were calculated (Beissner et al., 2010; Chung et al., 2015):

$$\begin{aligned} T_2*(t) &= (TE2 - TE1)/\ln(S_1(t)/S_2(t)), \\ S_0(t) &= S_1(t)^{TE2/(TE2-TE1)} S_2(t)^{TE1/(TE1-TE2)}, \end{aligned} \quad \text{eq. 3}$$

It should be mentioned that the amplitude of $S_0(t)$ also includes contributions from proton density, receiver sensitivity, and T_1 weighting. T_2* values that were negative or larger than

100 ms were omitted from further analysis. Baseline apparent T_1 maps were calculated by nonlinear least-squares curve-fitting the pre-steady state EPI images (Mazaheri et al., 2006) of TE1, i.e., the first epoch of each scan, using the formula:

$$M_{n+1}=\sin\alpha[M_0-(M_0-M_n\cos\alpha)e^{-TR/T1}], \quad \text{eq. 4}$$

where α is the flip angle and M_0 and M_n are the transverse magnetization after first and n-th excitation.

Once calculated according to Eq. [1] and Eq. [2], 16 laminar time-courses of BOLD, T_2*, and S_0 were combined into five anatomical layers (L 1 and 2, 3, 4, 5, and 6) according to the ratio of each layer's thickness to the whole cortical thickness in the marmoset's primary somatosensory cortex (S1) (Hardman and Ashwell, 2012), and then averaged across two hemisphere and all sessions. For better visualizing the temporal dynamics in L1+2, a normalized Gaussian weighted moving filter (full width at half maximum [FWHM] = 0.7 s) was applied to all three time-courses in L1+2. Session-averaged laminar responses were calculated by averaging the unfiltered time-courses from 2 s to 6 s after the stimulus onset and statistical tests were performed using one-sided paired t-tests. Laminar onset times were defined by the time to 10% peak of the hemodynamic response function (HRF) (Yen et al., 2011), which were generated by fitting each of the unfiltered time-courses of BOLD, T_2*, and S_0 with a linear combination of three gamma density functions (Friston et al., 1998) using nonlinear least-squares curve-fitting in Matlab. Onset time for layers without significant changes ($p > 0.05$) on session-averaged laminar responses were excluded. In addition, laminar time to peak and bandwidth were calculated by the time to 90% peak and the duration between 50% peak, i.e., FWHM of the same HRF. Timing values that ranked below 5% or beyond 95% of the whole dataset were treated as outliers and excluded from statistical tests. Balanced one-way analysis of variance (ANOVA) and post-hoc analysis of multiple paired t-tests were done using Matlab's anova1 and ttest functions, respectively.

Results

During fMRI experiments, marmosets were constantly monitored by an MR-compatible camera inside the magnet. The individualized 3D-printed helmet/chin pieces were very effective in providing comfortable yet effect head restraint, and for the vast majority of their time inside the magnet, the marmosets were resting with their eyes closed. Occasionally, they would open their eyes to check their surroundings or momentarily adjust their body position. Supplementary figure S1 shows an example session with five runs spanning over 86 minutes of scan time. Up to seven runs could be performed within each two-hour session, when the marmoset was completely compliant. When excessive head or body motion was detected, both MRI scans and stimuli were interrupted. The experiments were then allowed to resume after the marmosets were again relaxed. We ran a total of 21 sessions in four marmosets. Sessions with uncorrectable head movement (2/21), or those in which only unilateral activation was detected (5/21), were discarded from further analysis.

For the remaining 14 sessions included in the analysis, electrical stimulation of both hands induced robust positive BOLD responses in S1, in the secondary somatosensory cortex (S2), and in the caudate nucleus (Cd) of both hemispheres (Liu et al., 2013). Figure 1a shows a representative BOLD statistical t-map overlaid on the baseline anatomical image (TE = 27 ms) averaged over one entire session. To show the parcellation of cortical regions, the corresponding diagram taken from a marmoset brain atlas (Paxinos, 2012) was registered to the image and the boundaries of S1 (A3b), the external (S2E) and internal (S2I) portions of S2, and Cd are shown overlaid on the right hemisphere (Fig. 1a). Besides the robust activation of S1, S2, and Cd, significant BOLD responses can be also detected around primary auditory cortices (AuA1). We do not know the specific reasons for the activation of AuA1, as there were no specific sounds time-locked to the functional paradigm. One possibility is that the BOLD responses observed in AuA1 reflect activation of S2 being drained away via intracortical veins common to both S2 and AuA1. Another possibility is that BOLD responses in AuA1 originated from cross-modal activation of the somatosensory system (Fu et al., 2003).

Gray matter (GM) and white matter (WM) boundaries of both hemispheres were generated by second order polynomial fitting of manually defined cortical boundaries as shown in Fig. 1b. The second-order polynomial produced a smooth curvature, which disregarded artifacts caused by large pial veins shown on the right edge of the fitted curve. Please note that MR signal dropouts induced by the presence of pial veins were exaggerated in EPI images with long TE. In these cases, the hotspots of the BOLD activation maps in S1 were used to help define the true edge of the GM boundary on short TE EPI images. For each GM boundary point, projection lines orthogonal to the fitted gray matter boundary line were generated, as shown on the left hemisphere in Fig. 1b. Sixteen bi-linearly interpolated points along each projection line were grouped into five cortical layers (L1+2, L3, L4, L5, and L6) according to the atlas (Hardman and Ashwell, 2012) shown on the right hemisphere in Fig. 1b.

Time-courses of relative BOLD signal changes, absolute T_2* differences, and relative S_0 signal changes were extracted from the 16 profile points as defined above and averaged across sessions. The depth-dependent time-courses for each of the three different variables are shown in Fig. 2a, b, and c, respectively. Time-courses of the standard deviation for each measurement are displayed in Fig. 2d, e, and f. Higher variation of all three functional time courses was observed in L1+2 compared to other layers. As shown in Fig. 2a, positive BOLD signal changes were detected in all layers of the cortex. The largest BOLD signal changes were in L3 (0.4–0.8 mm below the pial surface), while the smallest changes occurred in L6. The onset of the positive BOLD response occurred 1–2 s after the onset of the stimulus, and the peak amplitude was reached 3–4 s after the onset of the stimulus. A noticeable post-stimulus undershoot was observed throughout the entire cortical depth from 10 s to 15 s after stimulus onset (Fig. 2a).

Unlike BOLD, absolute T2* differences in response to somatosensory stimulation were more spatially confined across the cortical depth (Fig. 2b). The largest ΔT_2* changes occurred in L3 from 0.6 mm to 0.8 mm below the cortical surface. However, the smallest ΔT_2* changes occurred in the most superficial layers of the cortex, L1+2 (top trace in Fig. 2e). Because of the small ΔT_2* changes in the most superficial layers, the major contributor

to the BOLD signal changes was the relative S_0 signal changes (Fig. 2c), which were highest at the cortical surface and negligible in all other layers of the cortex.

Figure 3 shows laminar profiles of baseline T_2*, S_0, and T_1, averaged across all sessions and all animals. The profiles include voxels from above the superficial gray matter boundary (cortical depth 0) to below the gray-white matter boundary (cortical depth 2.13 mm). The gray matter boundary point has higher T_2* than that of L1+2 owing to partial volume influences from the CSF-rich meninges. The T_2* (26.1 ± 4.1 ms) of superficial layers L1+2 was the lowest among all layers because the diameter of marmoset's pial vessels are around 90 μm (Guibert et al., 2010), and the thickness of cortical layers 1 and 2 are both less than 100 μm (Hardman and Ashwell, 2012), smaller than the imaging resolution (250 μm). Thus, L1+2 might be affected by the intravascular component of pial veins, which have T_2* ≈ 13 ms (Li et al., 2006). L1+2 might also be affected by the extravascular component of pial veins running perpendicular to the main magnetic field, which induce local susceptibility gradient up to six times larger than their own radius in radial direction when TE is chosen near the tissue T_2* (Park et al., 2008). T_2* values in layers 3–6 quickly recovered as a function of cortical depth (Fig. 3, blue trace). T_1 also exhibited a laminar dependent profile (Fig. 3, red trace). The highest values for T_1 were near the gray matter boundary, supporting the contribution of CSF. The values of T_1 throughout the cortical depth were relatively stable, but there were measurable local drops in T_1 at the border of L3 and L4, and near the white matter boundary, due to the higher myelination density in L4 and in white matter (Fig. 3). The laminar profile of S_0 (Fig. 3, green trace) has contributions from proton density, T_1, and from the receiver coil sensitivity profile. Because of these contributions, S_0 was highest in L1+2 and decreased monotonically with cortical depth.

Figure 4 shows the relative BOLD, relative T_2*, and relative S_0 response amplitudes at each of the five layers from L1+2 to L6. BOLD percent signal changes were highest in L1+2–L4 and smallest in L5 and L6. On the other hand, the highest relative T_2* percent changes were in L3–L4, stronger than in other layers of the cortex. Intriguingly, the relative S_0 response was significant only in L1+2 (~0.38%), but negligible elsewhere. This superficial S_0 functional response contributed significantly to the BOLD response in L1+2 (~1.33%), where the T_2* percent changes (~0.80%) could not fully account for the entire BOLD response.

To visualize onset time and time to peak, time-courses of the functional BOLD, T_2*, and S_0 changes were normalized and plotted in Fig. 5a, b, and c, respectively. Since there were no significant S_0 functional responses in layers other than L1+2, their normalized time-courses are not shown in Fig. 5c. The earliest BOLD responses (Fig. 5a) occurred in L3 and L4, followed by L1+2, L5, and L6. This is consistent with the expected flow of information from thalamus into the cortex (Ahissar and Staiger, 2010). Times to peak showed a similar trend as onset time. In Fig. 5b, onset time and time to peak of the T_2* time-courses in L1+2 could not be clearly visualized due to a high temporal variation originating from the lower T_2* baseline, which magnified physiological fluctuations during normalization of the functional time-courses. For the other layers, the earliest T_2* onset times occurred in L3 and L4, followed by L5 and L6.

For each of the three functional variables, the averaged time-course was fitted by summing three gamma density functions. Onset time, time to peak, and bandwidth were calculated for each of the five laminar regions from the fitted HRF and are summarized in Table 1. The BOLD onset times across the different layers were significantly different (ANOVA $p = 0.01$). Post-hoc paired t-tests revealed significant differences ($p < 0.05$) between L1+2 & L5, L1+2 & L6, L3 & L5, L3 & L6, L4 & L5, and L4 & L6. The onset time of upper layers (L1+2, L3, and L4) were significantly shorter than lower layers (L5 and L6). The T_2* onset times seemed to follow the trend of BOLD onset times, although no significant differences were found across the different layers (ANOVA $p = 0.59$). When comparing onset times within the same layer, T_2* had a significantly shorter onset time than BOLD at L3 (one-sided paired t-test, $p = 0.048$); S_0 had a significantly shorter onset time than T_2* at L1+2 (one-sided paired t-test, $p = 0.049$). Laminar analysis of time to peak for all three functional data showed a similar trend as for the onset time (Table 1). The p-value for ANOVA was 0.0002 and 0.04 for BOLD and T_2*, respectively. Post-hoc paired t-tests showed that time to peak of BOLD and T_2* were significantly different between L1+2 & L5 (not in T_2*), L1+2 & L6, L3 & L5, L3 & L6, L4 & L5, L4 & L6, and L5 & L6. But, no significant differences in time to peak could be found when comparing BOLD, T_2*, and S_0 within the same layer. The FWHM of BOLD and T_2* showed no significant differences between layers (ANOVA $p = 0.91$ for BOLD, 0.78 for T_2*), and no trends were observed across layers (Table 1), indicating that the FWHM of BOLD and T_2* changes were quite homogeneous across the cortical layers. When comparing FWHM of each layer between the three functional data, the T_2* FWHM in L3 was significantly longer than that of BOLD (one-sided paired t-test, $p = 0.011$), which was opposite to that of onset time.

Discussion

Sources of the non-deoxyHb component in superficial layers

In the present work, we show that the BOLD fMRI response to somatosensory stimulation has distinct and heterogeneous spatiotemporal characteristics across the layers of somatosensory cortex in awake marmosets. The largest and fastest BOLD signal changes were found in L1+2–L4, whereas the smallest and slowest responses were found in L5–L6 of the somatosensory cortex. The heterogeneous laminar distribution of the BOLD fMRI response was largely associated with changes in the deoxyHb component (T_2*) throughout most of the cortical depth, with the exception of the most superficial layers (L1+2), where the deoxyHb component alone did not account for the entire BOLD fMRI response. The most superficial layers were the only ones to show a non-negligible, non-deoxyHb component (S_0), and we estimate the contribution of S_0 to BOLD in L1+2 to be ~29%.

Functional changes in S_0 are mainly attributable to changes in both proton density and T_1, and an analysis of the possible sources of variation in both proton density and T_1 is necessary. First, it has been observed that T_1 is proportional to temperature and increases in tissue temperature due to increased neural activity (Coman et al., 2015). However, an increase in T_1 would result in a decrease in S_0. Furthermore, the temporal dynamics of changes in tissue temperature are significantly slower than the temporal dynamics of

changes in S_0 during functional hyperemia. Therefore, it is unlikely that the changes in S_0 observed in L1+2 are due to changes in brain tissue temperature.

Second, T_1 is known to be shortened by the inflow effect (Duyn et al., 1994), especially under conditions of large flip angle and short TR relative to the tissue T_1 (Glover et al., 1996). The inflow effect may be layer-dependent because most of the blood flowing in pial vessels runs perpendicular to the imaging plane (Guibert et al., 2010). Hence, the inflow effect contributes more to L1+2 than to the other layers. To properly estimate the contribution of inflow to S_0, we need to estimate the MR signal of arterial blood relative to the MR signal of brain tissue. Since we used a spatial saturation pulse below the circle of Willis, the blood signal can be calculated from a saturation recovery experiment. For this we had to estimate the arterial transit time (ATT) from the circle of Willis to the imaging plane. To the best of our knowledge, ATTs have not been reported for marmosets, but have been measured to be ~266 ms in rats (Thomas et al., 2006) and ~742 ms in macaques (Zappe et al., 2007). Therefore, we assumed the ATT in marmosets to be the average of these two species (504 ms). Assuming T_1 = 2.19 s (Li et al., 2015), and proton density relative to CSF = 0.83 (Leithner et al., 2010) for arterial blood, the blood signal arriving at the imaging plane at TE = 0 was calculated to be 0.170. The steady state incoherent (SSI) signals of the parenchyma at TE = 0 was calculated to be 0.180 by assuming T_1 = 1.83 (Bock et al., 2009), and proton density relative to CSF = 0.77 (Leithner et al., 2010) for the cortex. Hence, the signal from stationary spins in the cortex was larger than the signal from inflowing arterial water spins, indicating that the inflow effect was properly minimized or even contributed negatively. Most likely, the ATT in marmosets should be closer to the ATT in rats due to a similar body weight and heart rate. Under these conditions, the signal of incoming arterial blood would be 0.095, significantly smaller than the steady state signal of the cortex. Therefore, it is unlikely that inflow effect was the source of the observed S_0 increase in L1+2.

Third, both T_1 and proton density in L1+2 could decrease due to a simultaneous reduction of the CSF volume fraction and expansion of the parenchyma volume fraction crowding by enlargement of the cerebral blood volume (CBV) during functional hyperemia (Jin and Kim, 2010). To estimate the contribution of changes in the partial volume of CSF, SSI signals of CSF at TE = 0 were calculated as follows. Assuming T_1 = 4.43 s (Rooney et al., 2007), and proton density = 1 for CSF, the SSI signal of CSF is 0.137. SSI signals of the parenchyma were taken from the previous paragraph as 0.180. The average baseline CSF volume fraction has been reported to be 24.6% near the cortical surface, decreasing to 24.0% during functional hyperemia (Jin and Kim, 2010). Thus, the S_0 signal should increase 0.15%, which partially explains the 0.38% increase of S_0 in L1+2 reported here during somatosensory stimulation. Although the S_0 signal changes indirectly induced by CBV changes at L1+2 were small, they could justify the shorter onset time observed at L1+2. CBV changes have been reported to precede BOLD functional changes (Hirano et al., 2011; Jin and Kim, 2008; Shen et al., 2008), which is consistent with the shorter onset times of S_0 relative to those of T_2* by 0.2 s on average (Table 1). The delay of the deoxyHb component change in L1+2 might originate from the time oxygenated blood needed to travel from middle layers (0.5–1 mm) with venous flow velocity of 3–6 mm/s (Kennerley et al., 2010).

Last, a mono-exponential fitting might not perfectly describe the T_2* signal decay of either brain tissue (Whittall et al., 1999) or venous blood (Koopmans et al., 2011). For example, white matter, which was not included in the analysis, contains at least three compartments (van Gelderen et al., 2012). For gray matter in the middle of the cortex, fast and intermediate T_2 decay components, which account for 5% and 95% of the total signal, respectively, have been reported (He and Yablonskiy, 2007). Both of our echo times (13.5 ms and 40.5 ms) are much longer than the fast T_2* component of gray matter such that its contribution to our signal is marginal. In addition, the fraction of this fast T_2* component is small, which further minimizes its contribution to the signal. Under most fMRI experiments, TE is set to the T_2* value of gray matter, making this fast T_2* component invisible. While the intravenous and extravenous blood signal may be negligible in the parenchyma due to its tiny volume fraction (< 2.8%) (Kim and Kim, 2011) and small diameter (Guibert et al., 2010), it may be significant in the cortical surface (Jin et al., 2006) due to the presence of large pial veins (Guibert et al., 2010). Thus, a mono-exponential fitting of the MRI signal might overestimate S_0 in the cortical surface. The contribution of the intravenous and extravenous component to S_0 complements the contributions of changes in the partial volume of CSF estimated above at L1+2. It also implies that T_2* changes in our study are not contaminated by large pial veins, which are segregated into S_0 component.

Implications of mapping laminar T_2* changes by dual GR-EPI

When the inflow effect was suppressed, gradient echo BOLD responses in L1+2 no longer stood out compared to those in the middle layers. After segregating the T_2* effects surrounding pial veins and the CSF partial volume contribution, L1+2 showed significantly lower T_2* changes compared to those in the middle layers. The larger T_2* changes in layers 3 and 4 are correlated with the higher oxidative metabolic activities in both layers of S1 (Qi et al., 2008; Viaene et al., 2011). Therefore, T_2* changes are a surrogate measure of the underlying oxidative metabolic rate, which may be co-localized with laminar neural activity (Vazquez et al., 2012). As for the temporal characteristics, both layer 4 and the lower part of layer 3 of S1 receive dense afferents from ventroposterior nucleus of the thalamus, which relay hand stimuli to the cortices (Qi et al., 2008). Hence, layer 3 and 4 may exhibit shorter onset time compared to lower layers.

BOLD contrast is a multifaceted phenomenon, which consists of several factors other than change in blood oxygenation, including contributions from inflow effects, CSF and pial veins. Quantitative T_2* mapping may help segregate those artifacts and provide better insight to underlying neural activity (Kundu et al., 2014). Using a dual-echo GR-EPI sequence at 7T, we were able to map T_2* with a spatiotemporal resolution of 0.25x0.25x1 mm^3 and 200 ms. Laminar fMRI studies in parenchyma of healthy subjects will benefit by adopting high spatiotemporal resolution and dual echoes measurement.

Comparison of our results with the existing literature

It is interesting to compare the spatiotemporal heterogeneity of the laminar BOLD response observed here in awake marmosets with findings reported in other species. In 2002, Silva and Koretsky reported the highest amplitudes of the BOLD response to somatosensory stimulation in anesthetized rats to be in layers 1–3, followed by layers 4–5 and layer 6 (Silva

and Koretsky, 2002). The present data show the same trend if the cortical layers are combined in the same manner (data not shown). However, the laminar parcellation of the somatosensory cortex in rodents and primates is dramatically different. In S1, layers 1–3 occupy ca. 40% of the cortical thickness in rats, but ca. 55% in squirrel monkeys (Hutsler et al., 2005). Therefore, we could not follow the laminar parcellation previously used in rats. The laminar BOLD response patterns reported here are also corroborated by previous findings in anesthetized felines (Jin and Kim, 2008; Zhao et al., 2006). In those studies, the BOLD response was highest in the most superficial layers, with a relative contribution by pial veins of up to 60% (Jin et al., 2006; Kim and Ogawa, 2012). Under normal physiology, pial veins have shorter T_2* than tissue and the anesthesia agent used in those studies—isoflurane—significantly dilates blood vessels, resulting in an increased venous blood volume at baseline (Fukuda et al., 2013; Ohata et al., 1999) and amplification of the BOLD response in the most superficial layers. In the primary visual cortex of awake macaques, the highest BOLD response has been reported in the cortical surface due to contribution of pial veins (Chen et al., 2013). When large pial veins were excluded, the location of the maximum BOLD response occurred 0.6–0.8 mm in cortical depth (Chen et al., 2013). It is similar to the location of the maximum T_2* change in the current study, while contribution from pial veins was segregated into S_0. Therefore, using dual GR-EPI with TE near tissue T_2* actually might reduce large pial vein contamination from the cortical surface in laminar fMRI. Finally, when the cortical depth of the marmoset S1 was divided into three equal spaces (data not shown), our BOLD results were also comparable with findings from humans, which showed the highest BOLD response on the topmost voxel of the visual cortex (Siero et al., 2011). Comparison of finer laminar BOLD distribution would require performing higher spatial resolution fMRI in humans.

CBV-weighted fMRI has been suggested as a better modality to study the laminar hemodynamic response (Hirano et al., 2011; Jin and Kim, 2008; Kennerley et al., 2010; Shen et al., 2008; Zhao et al., 2006) because contamination from inflow effects and draining pial veins, which occur mostly on the superficial layers, are abolished by strong T_2* relaxation of the intravascular iron-oxide contrast agent under high magnetic field. Recently laminar CBV change was verified to co-localize with the highest neural activities in the olfactory bulb of rats (Poplawsky et al., 2015). It further encouraged us to conduct more experiments with CBV-weighted fMRI. In the meanwhile, iron-oxide contrast agent aided CBV-weighted fMRI has been demonstrated in awake rats (Luo et al., 2007) and awake macaques (Leite et al., 2002). We performed preliminary CBV-weighted fMRI experiments in awake marmosets (Hung et al., 2015a). Further investigations of CBV-weighted fMRI are underway to study the dynamics of the laminar hemodynamic response in awake marmosets.

Anesthetized rats show faster absolute onsets and slower absolute times-to-peak (Silva and Koretsky, 2002) than awake marmosets. One possible explanation is that anesthesia alters both baseline CBF and cerebrovascular reactivity (Leoni et al., 2011) such that the BOLD response is larger and lasts longer (Masamoto and Kanno, 2012). Hence, anesthesia may affect the amplitude and temporal dynamics of the fMRI response (Ferris et al., 2006; Liang et al., 2015). This was corroborated by a comparative study in awake and anesthetized marmosets showing the distinctive shape of HRF and inter-areal connectivity (Liu et al., 2013). Recently multi-unit recordings in the visual cortex of ferrets revealed that neural

activities at middle layer are significantly higher than other layers only under isoflurane anesthesia, but not during awake condition (Sellers et al., 2015). This potentially questions whether layer-dependent neural activity can be inferred from anesthetized animal models to awake humans. Therefore, studying the brain hemodynamic properties in awake marmosets without confounds of anesthesia might better reflect the hemodynamic features of the human brain (MacDonald et al., 2015) as well as the pathological changes in cerebrovascular disease (Traystman, 2016).

Limitations of the current study

It is essential to discuss the challenges and limitations of the current study. One challenge was to reliably determine the gray and white matter boundaries of the cortex so that we could do a proper segmentation of the cortical layers. Our approach was to determine the gray and white matter boundaries on the short TE images. When TE is chosen near the tissue T_2*, the susceptibility gradient induced by pial veins can impact T_2* values over a radial distance up to six times larger than their own radius (45 μm (Park et al., 2008). Because the short TE was half of the tissue T2*, however, the radius of the susceptibility gradient was approximately 162 μm, which was less than the in-plane resolution (250μm). This displacement was similar to the one caused by involuntary movements, such as pulsation and respiration. Therefore, using high resolution T_1 or T_2 anatomical images as references for laminar segmentation would not improve the laminar assignment, and thus we opted to use the short TE GR-EPI images as our reference for laminar segmentation.

Another challenge of the current study was to minimize artifacts induced by head motion, which are common when working with awake primates (Chen et al., 2012; Pfeuffer et al., 2007). The acclimation training and individualized 3D-printed helmets used here are quite effective in restricting head motion during fMRI experiments (Belcher et al., 2013; Hung et al., 2015c; Liu et al., 2013). The four marmosets used in the current study had passed the acclimation training and had been used for awake fMRI studies for more than three years. Two of the marmosets also went through the fixation training for visual fMRI and no incompliance issues were found (Hung et al., 2015b). However, still a small amount of head movement is inevitable in our experiments with awake animals. We relied on a combination of rigorous motion censoring (Power et al., 2014) and AFNI's motion correction (Cox and Hyde, 1997) to deal with motion artifacts. When marmosets moved more than half a voxel (125 μm) within one TR (200 ms), the images before and after the motion were excluded from further analysis (12% of all data). By using a combination of well-established acclimatization training procedures, individualized 3D-printed helmets, and robust motion censoring/correction, the impact of head motion to our data was greatly minimized.

Conclusions

A heterogeneous spatiotemporal distribution of relative BOLD signal changes in response to functional stimulation was observed across the layers of the primary somatosensory cortex in awake marmosets. The mid-upper cortical layers tended to have stronger relative BOLD signal changes and faster onset times than the lower ones. When the laminar BOLD signal changes were decomposed into their deoxyhemoglobin-related (absolute ΔT_2*) and

deoxyhemoglobin-unrelated (relative S_0 changes) components, the laminar ΔT_2* showed good spatiotemporal agreement with the corresponding BOLD signal changes in all layers except the most superficial ones, supporting the notion that changes in deoxyhemoglobin concentration are the predominant source of BOLD contrast. In the most superficial layers, relative S_0 changes were found to contribute roughly 29% to the BOLD changes and to have faster onset times than those of ΔT_2*. These superficial S_0 changes could not be explained by the inflow effect, which was minimized by spatial saturation of incoming blood, but may have originated from a functional reduction of CSF volume fraction and/or by unmodeled T_2* changes from extra- and intra-venous compartments within the cortical surface. Therefore, the spatiotemporal characteristics of laminar BOLD signal changes in L1+2 had contributions from changes in arterial blood volume and/or by pial veins near the cortical surface. The contribution from change in arterial blood volume may be reduced by nulling the CSF volume fraction with inversion pulses (Donahue et al., 2006; Scouten and Constable, 2008), while the influence of large veins to laminar BOLD change in the cortical surface may be mitigated by implementing spin-echo sequences (Lee et al., 1999; Yacoub et al., 2003). Caution should be taken when interpreting the increase of laminar BOLD fMRI as an increase of underlying neural activity in the most superficial layers if contributions from functional changes of inflow, CSF volume fraction, and large draining veins are present.

Supplementary Material

Refer to Web version on PubMed Central for supplementary material.

Acknowledgments

We thank Xianfeng (Lisa) Zhang, and Jennifer Lynn Ciuchta for their technical support in animal preparation. Also, many thanks go to the Scientific and Statistical Computing Core for their technical support in using AFNI to process the data. This research was supported by the Intramural Research Program of the NIH, NINDS (Alan P. Koretsky, Scientific Director).

References

Ahissar E, Staiger J. S1 laminar specialization. Scholarpedia. 2010; 5:7457.

Beissner F, Baudrexel S, Volz S, Deichmann R. Dual-echo EPI for non-equilibrium fMRI - implications of different echo combinations and masking procedures. Neuroimage. 2010; 52:524–531. [PubMed: 20420927]

Belcher AM, Yen CC, Stepp H, Gu H, Lu H, Yang Y, Silva AC, Stein EA. Large-scale brain networks in the awake, truly resting marmoset monkey. J Neurosci. 2013; 33:16796–16804. [PubMed: 24133280]

Bock NA, Kocharyan A, Liu JV, Silva AC. Visualizing the entire cortical myelination pattern in marmosets with magnetic resonance imaging. J Neurosci Methods. 2009; 185:15–22. [PubMed: 19737577]

Chen G, Wang F, Gore JC, Roe AW. Identification of cortical lamination in awake monkeys by high resolution magnetic resonance imaging. Neuroimage. 2012; 59:3441–3449. [PubMed: 22080152]

Chen G, Wang F, Gore JC, Roe AW. Layer-specific BOLD activation in awake monkey V1 revealed by ultra-high spatial resolution functional magnetic resonance imaging. Neuroimage. 2013; 64:147–155. [PubMed: 22960152]

Chung JY, Sung YW, Ogawa S. Evaluation of the Contribution of Signals Originating from Large Blood Vessels to Signals of Functionally Specific Brain Areas. BioMed Research International. 2015; 2015:6.

Coman D, Sanganahalli BG, Jiang L, Hyder F, Behar KL. Distribution of temperature changes and neurovascular coupling in rat brain following 3,4-methylenedioxymethamphetamine (MDMA, “ecstasy”) exposure. NMR Biomed. 2015; 28:1257–1266. [PubMed: 26286889]

Cox RW, Hyde JS. Software tools for analysis and visualization of fMRI data. NMR Biomed. 1997; 10:171–178. [PubMed: 9430344]

Cox RW, Jesmanowicz A, Hyde JS. Real-time functional magnetic resonance imaging. Magn Reson Med. 1995; 33:230–236. [PubMed: 7707914]

Donahue MJ, Lu H, Jones CK, Edden RA, Pekar JJ, van Zijl PC. Theoretical and experimental investigation of the VASO contrast mechanism. Magn Reson Med. 2006; 56:1261–1273. [PubMed: 17075857]

Duyn JH, Moonen CT, van Yperen GH, de Boer RW, Luyten PR. Inflow versus deoxyhemoglobin effects in BOLD functional MRI using gradient echoes at 1.5 T. NMR Biomed. 1994; 7:83–88. [PubMed: 8068530]

Ferris CF, Febo M, Luo F, Schmidt K, Brevard M, Harder JA, Kulkarni P, Messenger T, King JA. Functional magnetic resonance imaging in conscious animals: a new tool in behavioural neuroscience research. J Neuroendocrinol. 2006; 18:307–318. [PubMed: 16629829]

Friston KJ, Josephs O, Rees G, Turner R. Nonlinear event-related responses in fMRI. Magn Reson Med. 1998; 39:41–52. [PubMed: 9438436]

Fu KM, Johnston TA, Shah AS, Arnold L, Smiley J, Hackett TA, Garraghty PE, Schroeder CE. Auditory cortical neurons respond to somatosensory stimulation. J Neurosci. 2003; 23:7510–7515. [PubMed: 12930789]

Fukuda M, Poplawsky AJ, Kim SG. Submillimeter-resolution fMRI: Toward understanding local neural processing. Prog Brain Res. 2016; 225:123–152. [PubMed: 27130414]

Fukuda M, Vazquez AL, Zong X, Kim SG. Effects of the alpha(2)-adrenergic receptor agonist dexmedetomidine on neural, vascular and BOLD fMRI responses in the somatosensory cortex. Eur J Neurosci. 2013; 37:80–95. [PubMed: 23106361]

Glover GH, Lemieux SK, Drangova M, Pauly JM. Decomposition of inflow and blood oxygen level-dependent (BOLD) effects with dual-echo spiral gradient-recalled echo (GRE) fMRI. Magn Reson Med. 1996; 35:299–308. [PubMed: 8699940]

Goense J, Bohraus Y, Logothetis NK. fMRI at High Spatial Resolution: Implications for BOLD-Models. Front Comput Neurosci. 2016; 10:66. [PubMed: 27445782]

Guibert R, Fonta C, Plouraboue F. Cerebral blood flow modeling in primate cortex. J Cereb Blood Flow Metab. 2010; 30:1860–1873. [PubMed: 20648040]

Hardman, CD., Ashwell, KWS. Stereotaxic and chemoarchitectural atlas of the brain of the common marmoset (Callithrix jacchus). CRC Press; Boca Raton, FL: 2012.

He X, Yablonskiy DA. Quantitative BOLD: mapping of human cerebral deoxygenated blood volume and oxygen extraction fraction: default state. Magn Reson Med. 2007; 57:115–126. [PubMed: 17191227]

Hirano Y, Stefanovic B, Silva AC. Spatiotemporal evolution of the functional magnetic resonance imaging response to ultrashort stimuli. J Neurosci. 2011; 31:1440–1447. [PubMed: 21273428]

Hung C, Day-Cooney J, Russ B, Yen C, Notardonato L, Silva A, Leopold D. Neural responses to naturalistic movies in the common marmoset using electrocorticography and fMRI. Journal of Vision. 2015a; 15:580–580.

Hung CC, Yen CC, Ciuchta JL, Papoti D, Bock NA, Leopold DA, Silva AC. Functional mapping of face-selective regions in the extrastriate visual cortex of the marmoset. J Neurosci. 2015b; 35:1160–1172. [PubMed: 25609630]

Hung CC, Yen CC, Ciuchta JL, Papoti D, Bock NA, Leopold DA, Silva AC. Functional MRI of visual responses in the awake, behaving marmoset. Neuroimage. 2015c; 120:1–11. [PubMed: 26149609]

Hutsler JJ, Lee DG, Porter KK. Comparative analysis of cortical layering and supragranular layer enlargement in rodent carnivore and primate species. Brain Res. 2005; 1052:71–81. [PubMed: 16018988]

Jin T, Kim SG. Improved cortical-layer specificity of vascular space occupancy fMRI with slab inversion relative to spin-echo BOLD at 9.4 T. Neuroimage. 2008; 40:59–67. [PubMed: 18249010]

Jin T, Kim SG. Change of the cerebrospinal fluid volume during brain activation investigated by T(1rho)-weighted fMRI. Neuroimage. 2010; 51:1378–1383. [PubMed: 20338251]

Jin T, Wang P, Tasker M, Zhao F, Kim SG. Source of nonlinearity in echo-time-dependent BOLD fMRI. Magn Reson Med. 2006; 55:1281–1290. [PubMed: 16700023]

Kennerley AJ, Mayhew JE, Redgrave P, Berwick J. Vascular Origins of BOLD and CBV fMRI Signals: Statistical Mapping and Histological Sections Compared. Open Neuroimag J. 2010; 4:1–8. [PubMed: 20563253]

Kim SG, Ogawa S. Biophysical and physiological origins of blood oxygenation level-dependent fMRI signals. J Cereb Blood Flow Metab. 2012; 32:1188–1206. [PubMed: 22395207]

Kim T, Kim SG. Temporal dynamics and spatial specificity of arterial and venous blood volume changes during visual stimulation: implication for BOLD quantification. J Cereb Blood Flow Metab. 2011; 31:1211–1222. [PubMed: 21179068]

Koopmans PJ, Barth M, Orzada S, Norris DG. Multi-echo fMRI of the cortical laminae in humans at 7 T. Neuroimage. 2011; 56:1276–1285. [PubMed: 21338697]

Kundu P, Santin MD, Bandettini PA, Bullmore ET, Petiet A. Differentiating BOLD and non-BOLD signals in fMRI time series from anesthetized rats using multi-echo EPI at 11.7 T. Neuroimage. 2014; 102(Pt 2):861–874. [PubMed: 25064668]

Lee SP, Silva AC, Ugurbil K, Kim SG. Diffusion-weighted spin-echo fMRI at 9.4 T: microvascular/tissue contribution to BOLD signal changes. Magn Reson Med. 1999; 42:919–928. [PubMed: 10542351]

Leite FP, Tsao D, Vanduffel W, Fize D, Sasaki Y, Wald LL, Dale AM, Kwong KK, Orban GA, Rosen BR, Tootell RB, Mandeville JB. Repeated fMRI using iron oxide contrast agent in awake, behaving macaques at 3 Tesla. Neuroimage. 2002; 16:283–294. [PubMed: 12030817]

Leithner C, Muller S, Fuchtemeier M, Lindauer U, Dirnagl U, Royl G. Determination of the brain-blood partition coefficient for water in mice using MRI. J Cereb Blood Flow Metab. 2010; 30:1821–1824. [PubMed: 20842161]

Leoni RF, Paiva FF, Henning EC, Nascimento GC, Tannus A, de Araujo DB, Silva AC. Magnetic resonance imaging quantification of regional cerebral blood flow and cerebrovascular reactivity to carbon dioxide in normotensive and hypertensive rats. Neuroimage. 2011; 58:75–81. [PubMed: 21708273]

Li TQ, van Gelderen P, Merkle H, Talagala L, Koretsky AP, Duyn J. Extensive heterogeneity in white matter intensity in high-resolution T2*-weighted MRI of the human brain at 7.0 T. Neuroimage. 2006; 32:1032–1040. [PubMed: 16854600]

Li W, Grgac K, Huang A, Yadav N, Qin Q, van Zijl PC. Quantitative theory for the longitudinal relaxation time of blood water. Magn Reson Med. 2015

Liang Z, Liu X, Zhang N. Dynamic resting state functional connectivity in awake and anesthetized rodents. Neuroimage. 2015; 104:89–99. [PubMed: 25315787]

Liu JV, Hirano Y, Nascimento GC, Stefanovic B, Leopold DA, Silva AC. fMRI in the awake marmoset: somatosensory-evoked responses, functional connectivity, and comparison with propofol anesthesia. Neuroimage. 2013; 78:186–195. [PubMed: 23571417]

Luo F, Li Z, Treistman SN, Kim YR, King JA, Fox GB, Ferris CF. Confounding effects of volatile anesthesia on CBV assessment in rodent forebrain following ethanol challenge. J Magn Reson Imaging. 2007; 26:557–563. [PubMed: 17729349]

MacDonald AA, Naci L, MacDonald PA, Owen AM. Anesthesia and neuroimaging: investigating the neural correlates of unconsciousness. Trends Cogn Sci. 2015; 19:100–107. [PubMed: 25592916]

Marmoset Genome S, Analysis C. The common marmoset genome provides insight into primate biology and evolution. Nat Genet. 2014; 46:850–857. [PubMed: 25038751]

Masamoto K, Kanno I. Anesthesia and the quantitative evaluation of neurovascular coupling. J Cereb Blood Flow Metab. 2012; 32:1233–1247. [PubMed: 22510601]

Mazaheri Y, Biswal BB, Ward BD, Hyde JS. Measurements of tissue T1 spin-lattice relaxation time and discrimination of large draining veins using transient EPI data sets in BOLD-weighted fMRI acquisitions. Neuroimage. 2006; 32:603–615. [PubMed: 16713305]

Norup Nielsen A, Lauritzen M. Coupling and uncoupling of activity-dependent increases of neuronal activity and blood flow in rat somatosensory cortex. J Physiol. 2001; 533:773–785. [PubMed: 11410634]

Ohata H, Iida H, Dohi S, Watanabe Y. Intravenous dexmedetomidine inhibits cerebrovascular dilation induced by isoflurane and sevoflurane in dogs. Anesth Analg. 1999; 89:370–377. [PubMed: 10439750]

Papoti D, Yen CC, Mackel JB, Merkle H, Silva AC. An embedded four-channel receive-only RF coil array for fMRI experiments of the somatosensory pathway in conscious awake marmosets. NMR Biomed. 2013; 26:1395–1402. [PubMed: 23696219]

Park SH, Masamoto K, Hendrich K, Kanno I, Kim SG. Imaging brain vasculature with BOLD microscopy: MR detection limits determined by in vivo two-photon microscopy. Magn Reson Med. 2008; 59:855–865. [PubMed: 18383285]

Paxinos, G. The marmoset brain in stereotaxic coordinates. 1. Academic Press; London; Waltham, MA: 2012.

Pfeuffer J, Shmuel A, Keliris GA, Steudel T, Merkle H, Logothetis NK. Functional MR imaging in the awake monkey: effects of motion on dynamic off-resonance and processing strategies. Magn Reson Imaging. 2007; 25:869–882. [PubMed: 17451900]

Poplawsky AJ, Fukuda M, Murphy M, Kim SG. Layer-Specific fMRI Responses to Excitatory and Inhibitory Neuronal Activities in the Olfactory Bulb. J Neurosci. 2015; 35:15263–15275. [PubMed: 26586815]

Power JD, Mitra A, Laumann TO, Snyder AZ, Schlaggar BL, Petersen SE. Methods to detect, characterize, and remove motion artifact in resting state fMRI. Neuroimage. 2014; 84:320–341. [PubMed: 23994314]

Qi, H-X., Preuss, T., Kaas, J. Somatosensory Areas of the Cerebral Cortex: Architectonic Characteristics and Modular Organization-6.08. In: Gardner, E., Kaas, JH., editors. The Senses: A Comprehensive Reference. 2008. p. 142-169.

Rooney WD, Johnson G, Li X, Cohen ER, Kim SG, Ugurbil K, Springer CS Jr. Magnetic field and tissue dependencies of human brain longitudinal 1H2O relaxation in vivo. Magn Reson Med. 2007; 57:308–318. [PubMed: 17260370]

Scouten A, Constable RT. VASO-based calculations of CBV change: accounting for the dynamic CSF volume. Magn Reson Med. 2008; 59:308–315. [PubMed: 18228581]

Sellers KK, Bennett DV, Hutt A, Williams JH, Frohlich F. Awake vs. anesthetized: layer-specific sensory processing in visual cortex and functional connectivity between cortical areas. J Neurophysiol. 2015; 113:3798–3815. [PubMed: 25833839]

Shen Q, Ren H, Duong TQ. CBF, BOLD, CBV, and CMRO(2) fMRI signal temporal dynamics at 500-msec resolution. J Magn Reson Imaging. 2008; 27:599–606. [PubMed: 18219630]

Siero JC, Petridou N, Hoogduin H, Luijten PR, Ramsey NF. Cortical depth-dependent temporal dynamics of the BOLD response in the human brain. J Cereb Blood Flow Metab. 2011; 31:1999–2008. [PubMed: 21505479]

Siero JC, Ramsey NF, Hoogduin H, Klomp DW, Luijten PR, Petridou N. BOLD specificity and dynamics evaluated in humans at 7 T: comparing gradient-echo and spin-echo hemodynamic responses. PLoS One. 2013; 8:e54560. [PubMed: 23336008]

Silva AC, Koretsky AP. Laminar specificity of functional MRI onset times during somatosensory stimulation in rat. Proc Natl Acad Sci U S A. 2002; 99:15182–15187. [PubMed: 12407177]

Silva AC, Liu JV, Hirano Y, Leoni RF, Merkle H, Mackel JB, Zhang XF, Nascimento GC, Stefanovic B. Longitudinal functional magnetic resonance imaging in animal models. Methods Mol Biol. 2011; 711:281–302. [PubMed: 21279608]

Speck O, Hennig J. Functional imaging by I0- and T2*-parameter mapping using multi-image EPI. Magn Reson Med. 1998; 40:243–248. [PubMed: 9702706]

Sun T, Hevner RF. Growth and folding of the mammalian cerebral cortex: from molecules to malformations. Nat Rev Neurosci. 2014; 15:217–232. [PubMed: 24646670]

Thomas DL, Lythgoe MF, van der Weerd L, Ordidge RJ, Gadian DG. Regional variation of cerebral blood flow and arterial transit time in the normal and hypoperfused rat brain measured using

continuous arterial spin labeling MRI. J Cereb Blood Flow Metab. 2006; 26:274–282. [PubMed: 16034369]

Thomson AM, Bannister AP. Interlaminar connections in the neocortex. Cereb Cortex. 2003; 13:5–14. [PubMed: 12466210]

Tian P, Teng IC, May LD, Kurz R, Lu K, Scadeng M, Hillman EM, De Crespigny AJ, D'Arceuil HE, Mandeville JB, Marota JJ, Rosen BR, Liu TT, Boas DA, Buxton RB, Dale AM, Devor A. Cortical depth-specific microvascular dilation underlies laminar differences in blood oxygenation level-dependent functional MRI signal. Proc Natl Acad Sci U S A. 2010; 107:15246–15251. [PubMed: 20696904]

Traystman, RJ. Effect of Anesthesia in Stroke Models. In: Dirnagl, U., editor. Rodent Models of Stroke. Springer New York; New York, NY: 2016. p. 123-146.

van Gelderen P, de Zwart JA, Lee J, Sati P, Reich DS, Duyn JH. Nonexponential T(2) decay in white matter. Magn Reson Med. 2012; 67:110–117. [PubMed: 21630352]

Vazquez AL, Fukuda M, Kim SG. Evolution of the dynamic changes in functional cerebral oxidative metabolism from tissue mitochondria to blood oxygen. J Cereb Blood Flow Metab. 2012; 32:745–758. [PubMed: 22293987]

Viaene AN, Petrof I, Sherman SM. Properties of the thalamic projection from the posterior medial nucleus to primary and secondary somatosensory cortices in the mouse. Proc Natl Acad Sci U S A. 2011; 108:18156–18161. [PubMed: 22025694]

Whittall KP, MacKay AL, Li DK. Are mono-exponential fits to a few echoes sufficient to determine T2 relaxation for in vivo human brain? Magn Reson Med. 1999; 41:1255–1257. [PubMed: 10371459]

Yacoub E, Duong TQ, Van De Moortele PF, Lindquist M, Adriany G, Kim SG, Ugurbil K, Hu X. Spin-echo fMRI in humans using high spatial resolutions and high magnetic fields. Magn Reson Med. 2003; 49:655–664. [PubMed: 12652536]

Yen CC, Fukuda M, Kim SG. BOLD responses to different temporal frequency stimuli in the lateral geniculate nucleus and visual cortex: insights into the neural basis of fMRI. Neuroimage. 2011; 58:82–90. [PubMed: 21704712]

Yu X, Qian C, Chen DY, Dodd SJ, Koretsky AP. Deciphering laminar-specific neural inputs with line-scanning fMRI. Nat Methods. 2014; 11:55–58. [PubMed: 24240320]

Zappe AC, Reichold J, Burger C, Weber B, Buck A, Pfeuffer J, Logothetis NK. Quantification of cerebral blood flow in nonhuman primates using arterial spin labeling and a two-compartment model. Magn Reson Imaging. 2007; 25:775–783. [PubMed: 17490842]

Zhao F, Wang P, Hendrich K, Ugurbil K, Kim SG. Cortical layer-dependent BOLD and CBV responses measured by spin-echo and gradient-echo fMRI: insights into hemodynamic regulation. Neuroimage. 2006; 30:1149–1160. [PubMed: 16414284]

Highlights

- Deoxyhemoglobin-related and -unrelated fMRI responses examined in awake marmosets
- BOLD, T_2* and S_0 images were obtained in 5 laminar regions of somatosensory cortex
- The middle layers had the highest BOLD and T2* amplitudes and shortest onset times
- Functional S_0 changes were detected only in superficial layers with a fast onset time
- Basis of S_0 changes is likely changes in CBV and unmodeled T_2 * venous contributions

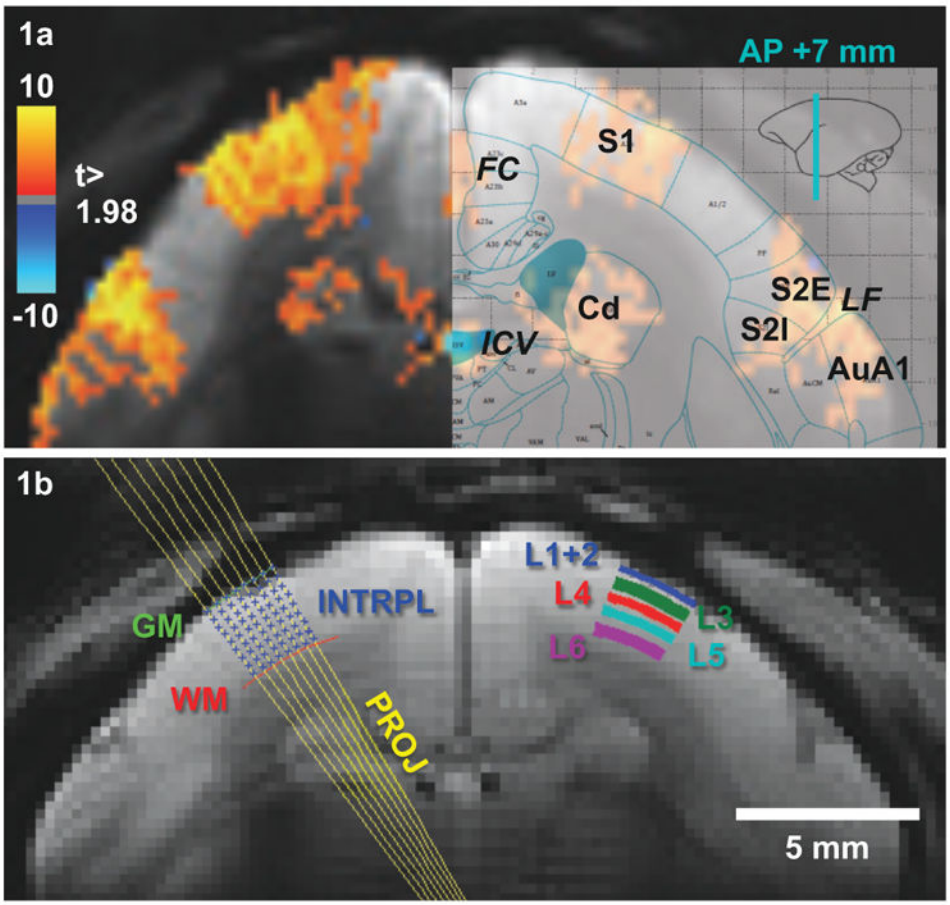

Fig. 1.

BOLD responses overlaid on the averaged EPI (TE = 27 ms) (a) and laminar segmentation (b) overlaid on the averaged EPI (TE = 13.5 ms) of one animal. (a) Robust BOLD responses were observed in S1, S2, and caudate of all animals. In addition, BOLD signals were seen in draining veins near FC and ICV as well as in AuA1. The slice position was determined from previous fMRI sessions and is located in AP +7 mm. (b) Gray and white matter boundaries were determined by second order polynomial fitting of manually defined white and gray matter edge points. Projection lines of each gray mater edge point were perpendicular to the gray matter boundary and bi-linear interpolated into 18 points (8 points shown here). Excluding 2 boundary points, 5 cortical layers were grouped from 16 interpolation points according to the histological layer definition. FC: falx cerebri, ICV: internal cerebral vein, Cd: caudate, LF: lateral fissure, S1: primary somatosensory cortex, S2E: external part of secondary somatosensory, S2I: internal part of secondary somatosensory, AuA1: primary auditory cortex, GM: gray matter boundary, WM: white matter boundary, INTRPL: interpolation points, PROJ: projection lines, L1 to L6: cortical layers 1 to 6.

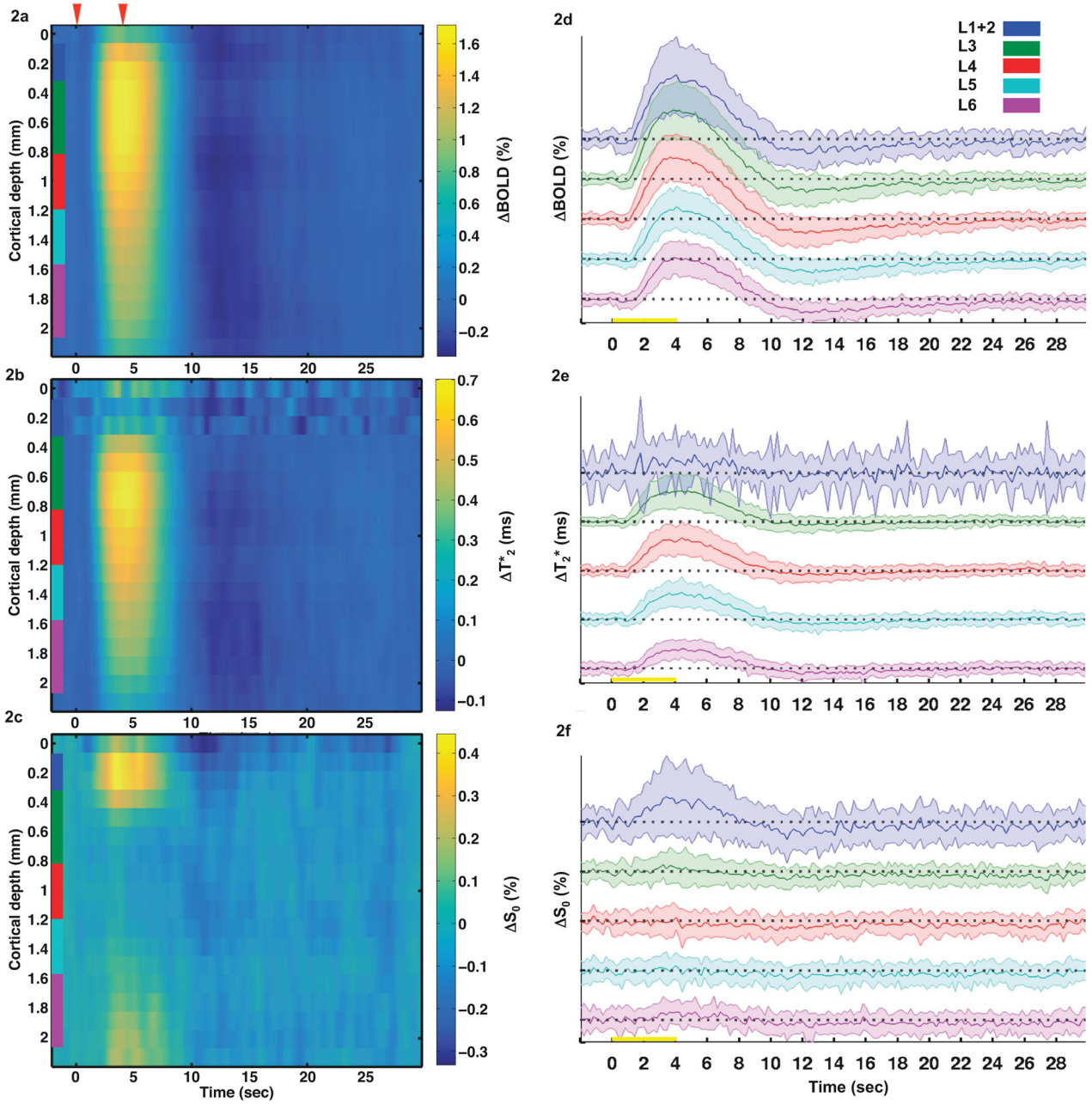

Fig. 2.

Laminar profiles and time-courses of relative BOLD changes (a, d), T_2* differences (b, e), and relative S_0 changes (c, f) over a single 32 s-long epoch. The magnitude and the onset time of the BOLD change were highest and fastest in L3-L4. A similar trend was observed in the ΔT_2* profile. On the other hand, S_0 changes were only observed in L1+2. Red arrows or yellow bars indicate the stimulus onset at t = 0 s and stimulus offset at t = 4 s. Color scales represent minimum to maximum intensity for each laminar profile. Laminar segmentation: L1+2 = blue, L3 = green, L4 = red, L5 = cyan, L6 = purple. Shaded curves

represent one standard deviation away from the averaged time-courses. The scale of the y-axis is percentage for ΔBOLD and ΔS_0 and millisecond for ΔT_2*, respectively.

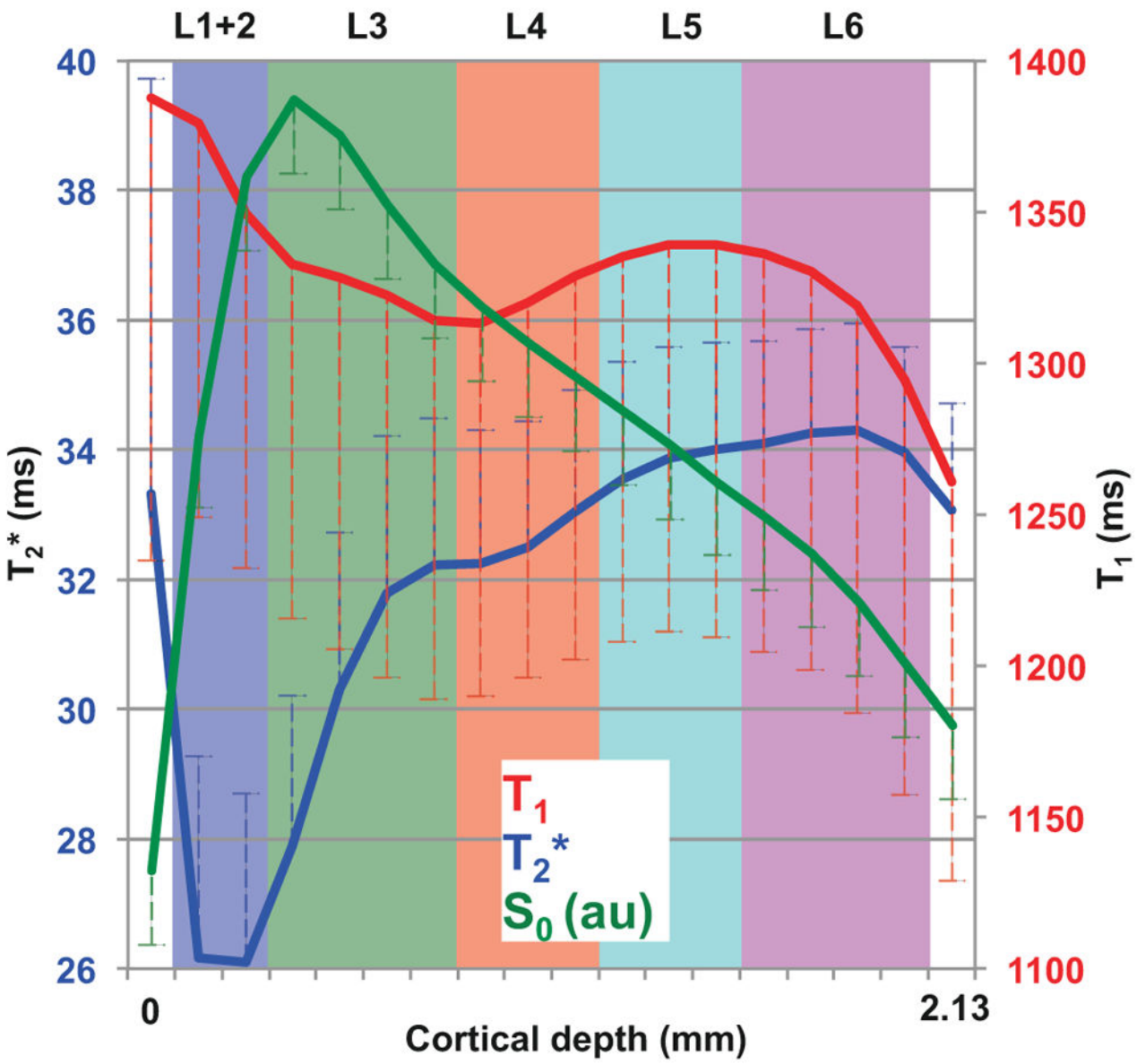

Fig. 3.

Baseline laminar profiles for T_2* (blue), T_{1app} (red), and S_0 (green). T_2* was lowest in L1+2 and showed a small dent around upper L4. T_1 was higher on superficial layers and showed a small dent at the same location as T_2*. S_0 increased sharply in the most superficial layers, peaked in the middle of L3, and decayed monotonically with the coil sensitivity profile along the cortical depth. The axis of S_0 is not shown in the plot since S_0 has arbitrary units. Error bars represent one standard deviation. Laminar segmentation: L1+2 = blue, L3 = green, L4 = red, L5 = cyan, L6 = purple.

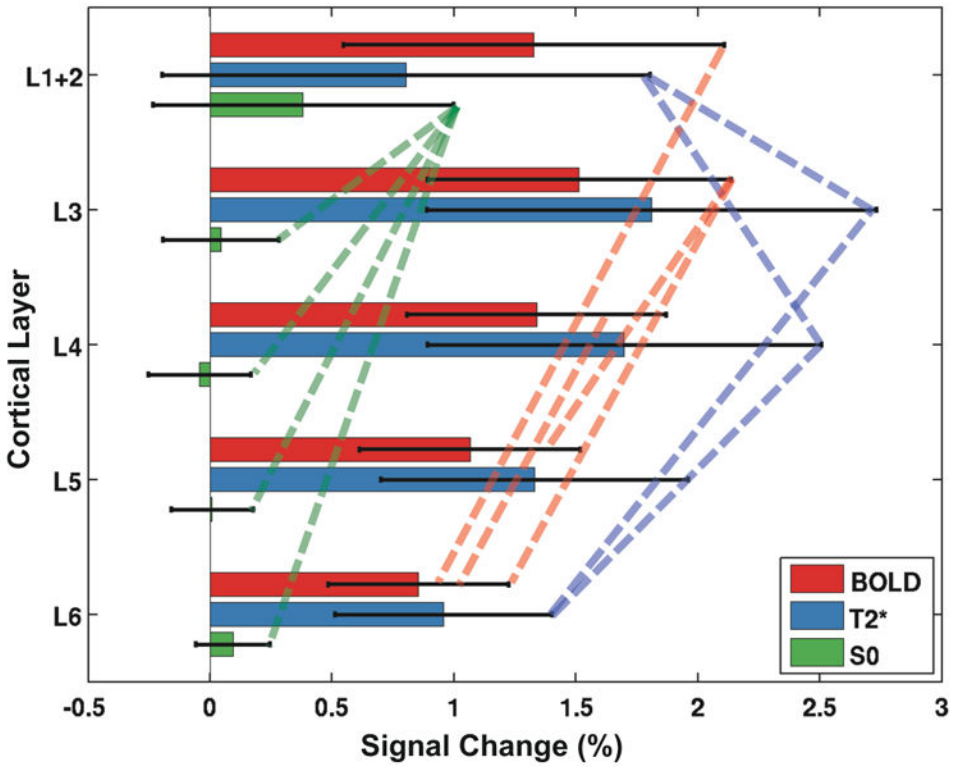

Fig. 4.

Averaged BOLD (red), T_2* (blue), and S_0 (green) percentage signal changes across the five laminar regions of S1. Significant ($t < 0.05$) BOLD and T_2* changes were detected in all five regions, whereas S_0 was only significantly different from baseline in L1+2. Additionally, BOLD changes were significantly different for some non-contiguous layer pairs as shown by red dot lines. For T2*, significant differences were observed in L1+2 compared to its adjacent layers (L3 and L4), which were also distinct from L6. Error bars represent one standard deviation. Significantly different pairs ($p < 0.05$) are connected with dashed lines.

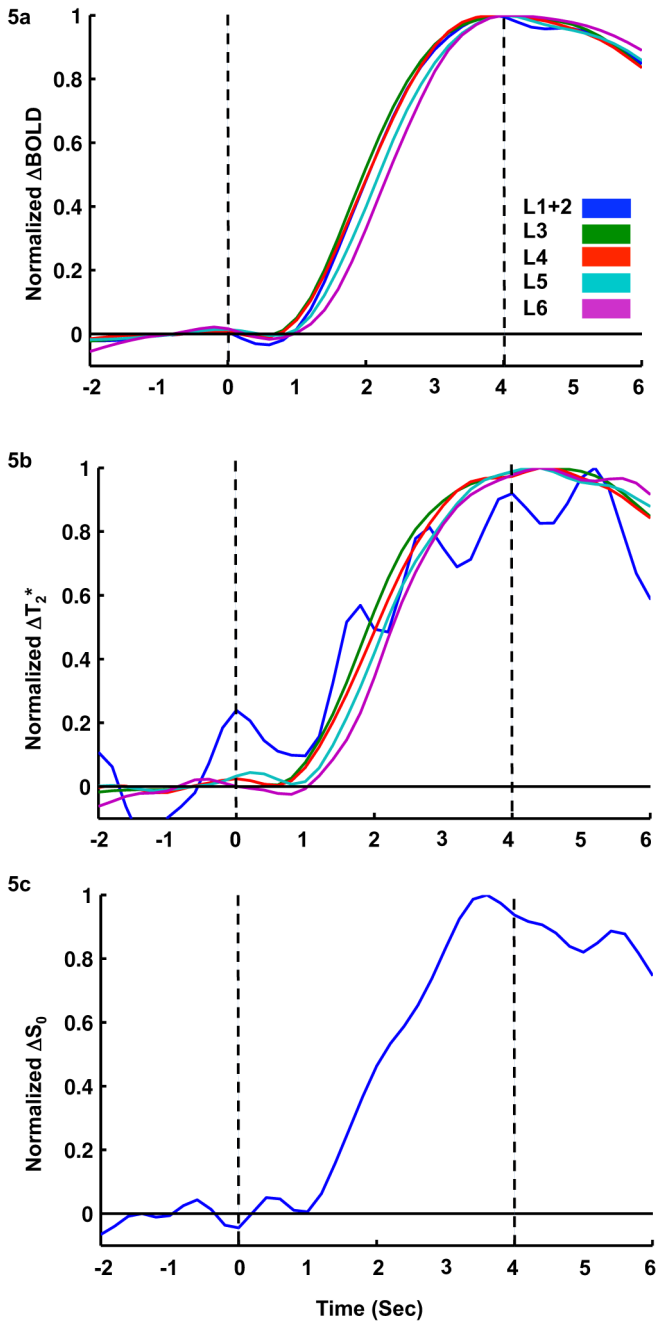

Fig. 5.

Peak-normalized laminar BOLD, T_2*, and S_0 time-courses. For laminar BOLD time-courses, the fastest onset times appeared in L3–L4, followed by L1+2, L5, and L6. For laminar T_2* time-courses, the ranking from BOLD was somewhat preserved besides L1+2, which was highly fluctuated. At L1+2, the onset time became obvious only when unfiltered time-courses were fitted with HRF of three gamma density functions. For laminar S_0 time-courses, only L1+2 was shown and analysis for onset time, because S_0 changes were only significant at L1+2.

Table 1

Temporal characteristics of the laminar BOLD, T_2*, and S_0 response in five laminar regions of S1. Times reported are mean ± standard deviation and the unit is second. P-values for ANOVA across five layers are 0.01, 0.59, 0.0002, 0.04, 0.91, and 0.78 for onset time of BOLD, onset time of T_2*, time to peak of BOLD, time to peak of T_2*, bandwidth of BOLD, and bandwidth of T_2*, respectively. n/a denotes insignificant response at this layer and hence no valid onset times are available. Underline color of laminar segmentation: L1+2 = blue, L3 = green, L4 = red, L5 = cyan, L6 = purple.

	Onset time			Time to peak			Bandwidth		
(Sec)	BOLD	T_2* deoxyHb	S_0	BOLD	T_2* deoxyHb	S_0	BOLD	T_2* deoxyHb	S_0
Layer 1+2	1.3±0.3	1.4±0.4	1.2±0.5	3.2±0.3	3.1±0.5	3.2±0.7	4.9±0.8	5.0±1.2	4.7±1.6
Layer 3	1.3±0.2	1.2±0.3	--	3.1±0.3	3.2±0.4	--	4.9±0.8	5.2±0.9	--
Layer 4	1.4±0.2	1.3±0.3	--	3.2±0.3	3.2±0.3	--	4.8±0.7	4.9±0.9	--
Layer 5	1.5±0.2	1.4±0.3	--	3.3±0.3	3.3±0.3	--	4.8±0.7	4.9±0.8	--
Layer 6	1.6±0.3	1.6±0.4	--	3.4±0.2	3.5±0.3	--	4.8±0.8	4.9±1.0	--